Optimization of Photodetector Thickness in Vertically-Integrated Image Sensors

Orit Skorka, Dan Sirbu, and Dileepan Joseph

Electrical and Computer Engineering, University of Alberta, Edmonton, AB, Canada

ABSTRACT

There is an emerging interest in vertically-integrated CMOS (VI-CMOS) image sensors. This trend arises from the difficulty in achieving high SNR, high dynamic range, and high frame rate with planar technologies while maintaining small pixel sizes, since the photodetector and electronics have to share the same pixel area and use the same technology. Fabrication methods for VI-CMOS image sensors add new degrees of freedom to the photodetector design. Having a model that gives a good approximation to the behavior of a device under different operating conditions is important for device optimization. This work presents a new approach in photodetector modeling, and uses it to optimize the thickness of the photosensitive layer in VI-CMOS image sensors. We consider a simplified structure of an a-Si:H photodetector, and develop analytical and numerical solutions, which are shown to be comparable, to state equations taken from semiconductor physics. If the photosensitive layer is too thin, our model shows that contact resistances dominate the device. If it is too thick, photogenerated carriers spread out too thinly and have little impact. Therefore, an optimum thickness can be found.

Keywords: active pixel sensor, thin film photodetector, hydrogenated amorphous silicon

1. INTRODUCTION

In many of their applications, image sensors are required to have high signal-to-noise ratio (SNR), high dynamic-range (DR), high resolution, and high frame rate. However, leading researchers have concluded that all these features cannot be achieved simultaneously with current planar technologies.[1] The various components in a typical image sensor can be categorized into two groups: optoelectronic devices and electronic circuits. The former includes the photodetectors, and the later includes the read-out, control and data processing circuits. The performance of each group is important for the overall performance of the image sensor. In monolithic CMOS, unlike CCD, various circuits can be designed to improve SNR and DR, but the photodetector and the electronics have to share the same pixel area. Moreover, photodetector optimization is impossible because the CMOS process, which is mainly used for memory and logic applications, cannot be fully optimized for imaging. Lastly, scaling down of the CMOS process may allow more pixel-level circuitry but as channel doping increases with the decrease in minimum feature size, the dark noise is also increased and this degrades photodetection.[2]

In recent years, there has been an increased interest in image sensors fabricated with three-dimensional structures, where the photodetectors are vertically integrated with the CMOS circuits. There are basically three technologies for fabrication of vertically-integrated CMOS (VI-CMOS) image sensors: thin film on ASIC (TFA),[3] stacked SOI,[4] and flip-chip assembly.[5] In VI-CMOS image sensors both the optoelectronics and the electronics can occupy the whole pixel area. But the main benefit of these fabrication methods is that the optoelectronics and the electronics can be optimized independently of each other. Consider that vertical integration allows more degrees of freedom than planar technologies in the design of the photodetector. For example, we are no longer restricted to crystalline silicon. Other semiconductors can be selected from considerations of desired detectable spectra, deposition conditions, and manufacturing capabilities and costs. Moreover, since the photodetectors can be fabricated in a process which is other than a standard CMOS one, their vertical thickness, which is determined in planar image sensors by diffusion profiles of the CMOS process, can now be varied.

The ability to predict the behavior of a semiconductor device under various operating conditions is important for the optimization of specific devices and their surrounding circuitry. The purpose of this work is to develop

orsk@ece.ualberta.ca, dil.joseph@ualberta.ca.

Sensors, Cameras, and Systems for Industrial/Scientific Applications X,
edited by Erik Bodegom, Valérie Nguyen, Proc. of SPIE-IS&T Electronic Imaging, SPIE Vol. 7249, 72490O
© 2009 SPIE-IS&T · CCC code: 0277-786X/09/$18 · doi: 10.1117/12.805999

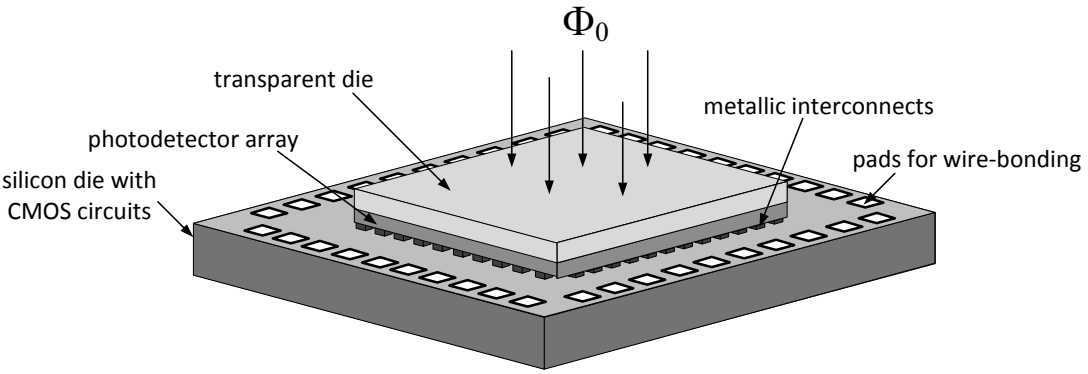

Figure 1. Schematic of an image sensor built with flip-chip assembly, one of the fabrication methods for VI-CMOS image sensors. A transparent die with an array of photodetectors is bonded through metallic interconnects to an array of read-out circuits on a silicon die. The silicon die, which is prepared in a standard CMOS process, also contains peripheral circuits and bond pads for external communication. Φ_0 refers to the incident illumination.

a model for one of the possible structures of a photodetector in VI-CMOS image sensors, and to use it for optimization of the thickness of the light-sensitive semiconductor layer in order to achieve a maximal contrast. Section 2 describes the simplified model of the photodetector, Section 3 presents the mathematical method that is used to solve the problem, Section 4 gives simulation results, and Section 5 reviews photodetectors reported in the literature, which were built with a structure similar to the one presented here. The method of solution, which was developed in this work, may be applied in future to different device structures and for different criteria of optimization.

2. THE PHOTODETECTOR MODEL

2.1 Photodetector structure

Fig. 1 illustrates a VI-CMOS image sensor made by flip-chip technology. In this fabrication method, the image sensor is composed of two dies: a transparent die with the photodetectors and a silicon die with the CMOS circuits. Each die is processed independently, to optimize performance, and as the last step they are aligned precisely and finally attached through metallic interconnects. The presented model is demonstrated for a photodetector structure intended for such a fabrication method.

In order to simplify the analysis, a one-dimensional approach is taken, where the device is assumed to be uniform in the other two dimensions. The schematic of the structure of this photodetector is shown in Fig. 2(a). It is composed of three layers, which are deposited in the following order on a transparent substrate, such as glass: a thin film of transparent-conductive oxide (TCO), a semiconductor layer with thickness ℓ, and a thin film of metal. The TCO forms the front contact, while allowing the illumination, Φ_0, to pass to the semiconductor, and the metal layer forms the electrical contact between the semiconductor and the CMOS read-out circuits. The semiconductor is the light-sensitive layer. The voltage across the photodetector is kept constant at V_{ab}, and J represents the current density through the device.

2.2 Problem statement

The optimal thickness for the photodetector, ℓ_{opt}, is defined as the thickness for which the contrast, β, is maximal. β is the ratio between J_{ph}, the current density under illumination, and J_{dk}, the current density in the dark, i.e.

$$\beta = \frac{J_{ph}}{J_{dk}}. \tag{1}$$

β reaches a maximum value when ℓ is varied because, as shown by our model, a too thin or too thick semiconductor layer has a disadvantage that leads to a low contrast ratio. If ℓ is made too thin, the resistance of the semiconductor, which decreases with illumination, would be lower than those of the metal-semiconductor and

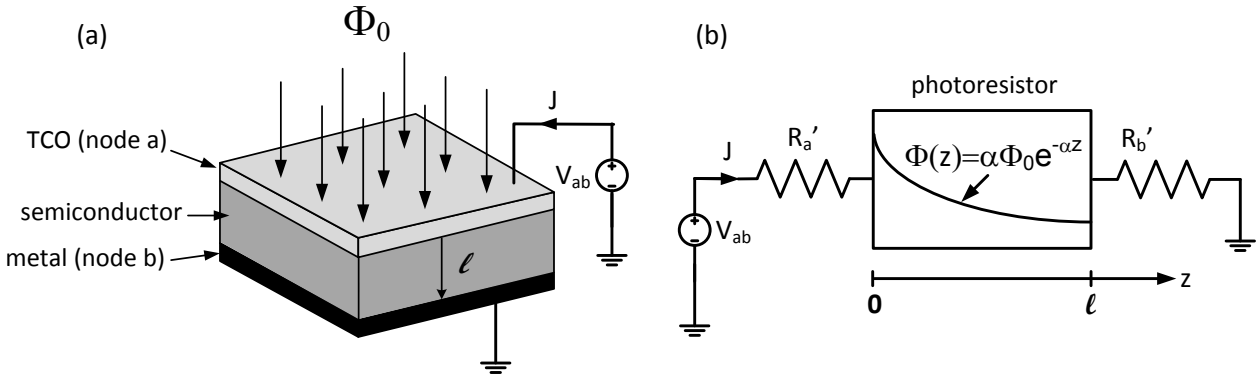

Figure 2. (a) A photodetector in a VI-CMOS image sensor. A semiconductor layer with thickness ℓ is sandwiched between two conductive layers: a transparent conductive oxide (TCO) (node a) and a metal (node b). The TCO forms a front contact while allowing the illumination, Φ_0, to reach the semiconductor; and the metal layer forms an electrical contact with the read-out circuits. The applied voltage across the TCO and metal layers is V_{ab}, and J is the current density. (b) A simplified electrical model for the photodetector. Contact resistances between the semiconductor and the two conductors are taken to be purely ohmic. Therefore, the whole device can be presented as three resistors in series. R'_a and R'_b are the scaled contact resistances (in $\Omega\,\mathrm{cm}^2$) between the TCO and semiconductor and the metal and semiconductor, respectively. The illumination decays exponentially as it is absorbed in the semiconductor. Since the absorbed photons generate free charge carriers that improve conductivity, the semiconductor is referred to as a *photoresistor*.

TCO-semiconductor contacts. This would result in an insignificant change in the current under illumination and, therefore, low β. If the semiconductor is made too thick, free charge carriers, which are generated by the absorption of the incident light, would diffuse further into the material and, in equilibrium, would be thinly distributed. This would result in an insignificant change in conductivity under illumination and, as before, would reduce β.

2.3 Three-resistor model

In order to work with a linear system, which simplifies the modeling and analysis, the two Schottky contacts between the semiconductor and the conductors are replaced with the equivalent resistance of these diodes around a nominal bias point. Therefore, the photodetector can be treated as a network of three serially-connected resistors, as shown in Fig. 2(b). R'_a and R'_b stand for the equivalent resistance, in $\Omega\,\mathrm{cm}^2$, of the junction between the semiconductor and the TCO and the junction between the semiconductor and the metal, respectively. The resistance of the bulk semiconductor decreases with the intensity of the illumination, Φ_0, because the absorbed light generates free charge carriers. This layer can therefore be referred to as a *photoresistor*. If a constant voltage, V_{ab}, is applied to the three-resistor network, the current density, J, will increase with increasing Φ_0.

2.4 Kirchoff's law and the electric field

Kirchoff's voltage law for the three-resistor network can be written as

$$V_{ab} = J \cdot (R'_a + R'_b) + V(0) - V(\ell) = J \cdot (R'_a + R'_b) + \int_0^\ell E(z)dz, \tag{2}$$

where E is the electric-field profile of the photoresistor. It depends on V, the potential inside the photoresistor, in the following way:

$$E(z) = -\frac{dV(z)}{dz}. \tag{3}$$

At each point along the z axis, E can be presented as a sum of its average value, E_{ext}, and a local perturbation, E_{int}, i.e.

$$E(z) = E_{ext} + E_{int}(z), \tag{4}$$

where

$$E_{ext} = \frac{1}{\ell}\int_0^{\ell} E(z)dz, \tag{5}$$

and

$$\int_0^{\ell} E_{int}(z)dz = 0. \tag{6}$$

Consequently, Eq. 2 may be rewritten as

$$V_{ab} = J \cdot (R'_a + R'_b) + \ell \cdot E_{ext}. \tag{7}$$

E, the total electric field in the semiconductor is a result of two factors: (i) the external applied voltage; and (ii) local differences in the concentration of charge carriers, which arise because charged particles travel with different mobilities. E_{ext} comes from the former factor, and E_{int} comes from the latter one. In general, the internal field is expected to be much smaller than the external one, and, therefore, is often neglected in hand calculations.[6] Later, the expressions for both fields are developed according to semiconductor physics and the problem is solved both analytically and numerically. For the analytical solution only E_{ext} is considered, and for the numerical solution E_{int} is also calculated. The simulation results show that E_{int} can indeed be neglected. Nonetheless, the approach we take to solve for E_{ext} and E_{int}, e.g. using Kirchoff's voltage law as a boundary condition, is different from the literature.

2.5 Charge carrier equations

Several processes occur simultaneously in the light-sensitive semiconductor. During their lifetime between generation and recombination, free charge carriers are subject to electric field, which drifts them to the contacts, and diffusion that forces them to overcome differences in concentration. To fully determine the steady state of the semiconductor layer under different conditions, one needs to solve a set of simultaneous equations. This set includes Poisson's equation, i.e.

$$\frac{dE(z)}{dz} = \frac{q}{\epsilon}\big(p(z) - n(z) + N_D^+(z) - N_A^-(z)\big), \tag{8}$$

and the continuity equations for holes and electrons, i.e.

$$\frac{dJ_p(z)}{dz} = q\big(g(z) - r(z)\big), \tag{9}$$

$$\frac{dJ_n(z)}{dz} = -q\big(g(z) - r(z)\big). \tag{10}$$

$\epsilon = \epsilon_0\epsilon_r$ is the dielectric constant of the semiconductor, q is the fundamental charge, p and n are the concentrations of holes and electrons, respectively, and N_D^+ and N_A^- are the densities of ionized donors and acceptors. g is the generation rate of charge carriers in the semiconductor and r is their recombination rate. J_p and J_n are the hole and electron current densities, which are given by the drift-diffusion equations, i.e.

$$J_p(z) = q\mu_p p(z)E(z) - qD_p\frac{dp(z)}{dz}, \tag{11}$$

and

$$J_n(z) = q\mu_n n(z)E(z) + qD_n\frac{dn(z)}{dz}. \tag{12}$$

μ_p and μ_n are hole and electron mobilities in the semiconductor, and D_p and D_n are the corresponding diffusion coefficients.

Considering only direct recombination at this stage, we have

$$r(z) = \alpha_r p(z) n(z), \tag{13}$$

where α_r is the bimolecular recombination coefficient. The generation includes both an optical generation process, g_{opt}, and a thermal generation process, g_{th}. The overall generation rate is given by

$$g(z) = g_{opt}(z) + g_{th}(z) = \int_0^\infty \alpha(\lambda)\Phi_0(\lambda)T(\lambda)e^{-\alpha(\lambda)z}d\lambda + \alpha_r p_0 n_0, \tag{14}$$

where p_0 and n_0 are the hole and electron concentrations in the dark, respectively, α is the absorption coefficient of the semiconductor at wavelength λ, and T is the percentage of such light transmitted into the semiconductor through the transparent substrate and TCO. Reflections from the metal contact are ignored for simplicity. For monochromatic light, Eq. 14 reduces to

$$g(z) = \alpha\Phi_0 T e^{-\alpha z} + \alpha_r p_0 n_0, \tag{15}$$

where $\Phi_0(\lambda)$ and Φ_0 in Eqs. 14 and 15 have different units ($\mathrm{cm^{-2}\,s^{-1}nm^{-1}}$ and $\mathrm{cm^{-2}\,s^{-1}}$, respectively).

3. THE MATHEMATICAL METHOD

The solution process is based on the mean values of the different variables in the semiconductor, and on the deviation of the local quantity from its mean value, which is similar to the way the electric field was treated in Section 2.4.

3.1 Excess charge carriers

The local concentration of either holes or electrons can be presented as a summation of its concentration in the dark, p_0 or n_0, and the concentration of excess charge carriers, δp or δn, due to light absorption, i.e.

$$p(z) = p_0 + \delta p(z), \tag{16}$$
$$n(z) = n_0 + \delta n(z). \tag{17}$$

Furthermore, the excess charge carriers can be presented as a sum of an average value, $\overline{\delta p}$ and $\overline{\delta n}$, and a local perturbation, γ_p and γ_n, for holes and electrons, respectively, i.e.

$$\delta p(z) = \overline{\delta p} + \gamma_p(z), \tag{18}$$
$$\delta n(z) = \overline{\delta n} + \gamma_n(z), \tag{19}$$

where

$$\overline{\delta p} = \frac{1}{\ell}\int_0^\ell \delta p(z)dz, \tag{20}$$
$$\overline{\delta n} = \frac{1}{\ell}\int_0^\ell \delta n(z)dz, \tag{21}$$

and

$$\int_0^\ell \gamma_p(z)dz = 0, \tag{22}$$
$$\int_0^\ell \gamma_n(z)dz = 0. \tag{23}$$

Consequently, one can derive the following:

$$\overline{p} = \frac{1}{\ell}\int_0^\ell p(z)dz = p_0 + \overline{\delta p}, \tag{24}$$

$$\overline{n} = \frac{1}{\ell}\int_0^\ell n(z)dz = n_0 + \overline{\delta n}, \tag{25}$$

which leads to the formulations:

$$p(z) = \overline{p} + \gamma_p(z), \tag{26}$$

$$n(z) = \overline{n} + \gamma_n(z). \tag{27}$$

While hole and electron concentrations are typically expressed as in Eqs. 16 and 17, we have reformulated them in terms of local perturbations because we found that it simplifies analysis and proves more robust numerically.

3.2 Conductivity and current density

The local conductivity of the semiconductor, σ, is given by

$$\sigma(z) = q\big(\mu_p p(z) + \mu_n n(z)\big). \tag{28}$$

Therefore, its mean value, $\overline{\sigma}$, can be written as

$$\overline{\sigma} = \frac{1}{\ell}\int_0^\ell \sigma(z)dz = q(\mu_p\overline{p} + \mu_n\overline{n}). \tag{29}$$

Furthermore, $\overline{\sigma}$ may be expressed as a sum of the dark conductivity, σ_{dk}, and the mean value, $\overline{\sigma}_{ph}$, of the change in conductivity when the photoresistor is illuminated ($\Phi_0 > 0$), i.e.

$$\overline{\sigma} = \sigma_{dk} + \overline{\sigma}_{ph}, \tag{30}$$

where

$$\sigma_{dk} = q(\mu_p p_0 + \mu_n n_0), \tag{31}$$

and

$$\overline{\sigma}_{ph} = q(\mu_p\overline{\delta p} + \mu_n\overline{\delta n}). \tag{32}$$

According to Kirchoff's current law, the current inside the semiconductor must be constant for all z and must equal J. Since this current density is composed of hole and electron contributions, i.e. J_p and J_n, one can write

$$J_p(z) + J_n(z) = J. \tag{33}$$

Therefore, J may be expressed as a mean value, i.e.

$$J = \frac{1}{\ell}\int_0^\ell \big(J_p(z) + J_n(z)\big)dz. \tag{34}$$

By applying Eqs. 11 and 12 to Eq. 34, one can rewrite J as

$$J = J_{ext} + J_{int}, \tag{35}$$

where

$$J_{ext} = \overline{\sigma}\cdot E_{ext}, \tag{36}$$

and

$$J_{int} = \frac{q}{\ell}\int_0^{\ell}\Big\{\big(\mu_p\gamma_p(z)+\mu_n\gamma_n(z)\big)E_{int}(z) - D_p\frac{d\gamma_p(z)}{dz} + D_n\frac{d\gamma_n(z)}{dz}\Big\}dz \tag{37}$$

or

$$J_{int} = \frac{q}{\ell}\Big\{\int_0^{\ell}\big(\mu_p\gamma_p(z)+\mu_n\gamma_n(z)\big)E_{int}(z)dz - D_p\big(\gamma_p(\ell)-\gamma_p(0)\big) + D_n\big(\gamma_n(\ell)-\gamma_n(0)\big)\Big\}. \tag{38}$$

By applying Eqs. 35 and 36 to Eq. 7, i.e. Kirchoff's voltage law for Fig. 2(b), J can be written as

$$J = \frac{V_{ab} + J_{int}\cdot\ell/\overline{\sigma}}{R'_a + R'_b + \ell/\overline{\sigma}}, \tag{39}$$

where $\ell/\overline{\sigma}$ is basically the scaled resistance of the photoresistor. One can conclude from Eq. 39 that the system actually has two voltage sources. The first is the applied voltage, V_{ab}, and the second is a voltage developed due to optical excitation of the semiconductor, i.e. $J_{int}\cdot\ell/\overline{\sigma}$.

3.3 Boundary conditions

To solve the system of charge carrier equations, which was presented in Section 2.5, one has to provide appropriate boundary conditions. In the literature, boundary conditions are often defined in terms of the concentration of charge carriers and current densities on the boundaries (see for example De Mari[7] and Gummel[8]). We found these boundary conditions did not work for our photodetector model and so developed new ones that not only work but also have a simpler interpretation.

The first boundary condition, presented in integral form in Eq. 2, is Kirchoff's voltage law. It incorporates the applied voltage, V_{ab}. The second boundary condition is charge neutrality. The material is initially neutral, and each generation or recombination process involves two particles: a hole and an electron. Therefore, the sum of excess charge carriers in the semiconductor must be zero, i.e.

$$\int_0^{\ell}\big(\delta p(z) - \delta n(z)\big)dz = 0. \tag{40}$$

Since $p_0 = N_A^-$ and $n_0 = N_D^+$, Eq. 8 reduces to

$$\frac{dE_{int}(z)}{dz} = \frac{q}{\epsilon}\big(\delta p(z) - \delta n(z)\big), \tag{41}$$

and so charge neutrality implies

$$E_{int}(0) = E_{int}(\ell). \tag{42}$$

Considering Eqs. 18 to 23, charge neutrality also implies

$$\overline{\delta p} = \overline{\delta n}, \tag{43}$$

which means Eq. 41 can be reduced to

$$\frac{dE_{int}(z)}{dz} = \frac{q}{\epsilon}\big(\gamma_p(z) - \gamma_n(z)\big). \tag{44}$$

For a more complex recombination process, Eq. 40 becomes more complicated (for example, it might include trapped charge carriers). However, the overall charge neutrality must be maintained.

The third boundary condition is generation-recombination balance. In the steady state, every electron-hole pair generation must be offset by electron-hole pair recombination. This is achieved by the condition

$$\int_0^{\ell}\big(g(z) - r(z)\big)dz = 0. \tag{45}$$

Considering Eqs. 13, 15, and 24 to 27, generation-recombination balance implies

$$\int_0^\ell \left\{ \alpha\Phi_0 T e^{-\alpha z} + \alpha_r p_0 n_0 - \alpha_r \big(p_0 + \overline{\delta p} + \gamma_p(z)\big) \cdot \big(n_0 + \overline{\delta n} + \gamma_n(z)\big) \right\} dz = 0. \tag{46}$$

When Eq. 43 is used, Eq. 46 can be rewritten in the following way

$$\alpha_r \overline{\delta n}^{\,2} + \alpha_r (p_0 + n_0)\overline{\delta n} - \frac{\Phi_0 T(1 - e^{-\alpha\ell})}{\ell} + \frac{\alpha_r}{\ell} \int_0^\ell \gamma_p(z)\gamma_n(z) dz = 0 \tag{47}$$

If $\gamma_p(z)$ and $\gamma_n(z)$ are known, Eq. 47 becomes a quadratic equation, from which $\overline{\delta n}$ can be derived. E_{int} can then be obtained from Eqs. 6 and 44, J_{int} is deducible from Eq. 38, and so on for the rest of the variables.

4. OPTIMIZATION OF THICKNESS

4.1 Solution process

For the analytical solution, it is assumed that the concentration of charge carriers in the semiconductor is uniform along the z axis, or in other words there is no perturbation, i.e. $\gamma_p = \gamma_n = 0$. In this case Eq. 47 has a single unknown, $\overline{\delta n}$, and E_{int} and J_{int} both vanish. In the dark ($\Phi_0 = 0$) there are no excess charge carriers and so $\overline{\delta n} = 0$ by Eq. 47, which means $\overline{\sigma}_{ph} = 0$ and the current density is given by

$$J_{dk} = J(\Phi_0 = 0) = \frac{V_{ab}}{R'_a + R'_b + \ell/\sigma_{dk}}. \tag{48}$$

The photocurrent is defined as the difference between the current under illumination and the current in the dark, i.e.

$$J_{ph} = J - J_{dk}. \tag{49}$$

If all material parameters and operating conditions are given, $\overline{\sigma}_{ph}$ and J can be readily calculated for any $\Phi_0 > 0$, and one can finally calculate the contrast, β, as defined in Eq. 1.

A numerical solution was also developed based on a finite-differences method.[9] It calculates γ_p and γ_n in an iterative way. The numerical solution is initialized with the quantities of the different variables when γ_p and γ_n are taken to be zero, i.e. the analytical solution. The overall results of the numerical solution are very similar to those that are obtained by the analytical one, which shows that the latter is very good. However, the numerical solution also allows calculation of the perturbation in the charge carrier concentrations, γ_p and γ_n, as well as the internal field, E_{int}, and the internal current density, J_{int}.

4.2 Shockley-Read-Hall recombination

The simulation was performed with material parameters of an intrinsic hydrogenated amorphous-silicon (a-Si:H) film, based on a plasma-enhanced chemical-vapor-deposition (PECVD) fabrication method. This material was chosen since it has been widely used for photodetection devices in the visible band, and, furthermore, it has been used in VI-CMOS image sensors.[3]

To agree with the physics of the material, the charge carrier equations had to be revised. In a-Si:H films, the recombination mechanism is dominated by the Shockley-Read-Hall (SRH) process. Although the actual SRH recombination process in a-Si:H is best described by a multi-level traps model, we use a simplified single-level trap SRH mechanism as presented by Sakata *et al.*[10] As the rest of the solution process proceeds in a manner similar to that described for direct recombination, we preferred to base Sections 2 and 3 on the simpler recombination model. With SRH, the recombination rate of the free charge carriers is given by (instead of Eq. 13)

$$r(z) = \alpha_r p(z) n(z) + \frac{p(z)n(z) - n_i^2}{\tau_p\big(n(z) + n_i\big) + \tau_n\big(p(z) + n_i\big)}, \tag{50}$$

where τ_p and τ_n are the recombination lifetimes of holes and electrons, respectively, and n_i is the intrinsic carrier concentration ($n_i^2 = p_0 n_0$).

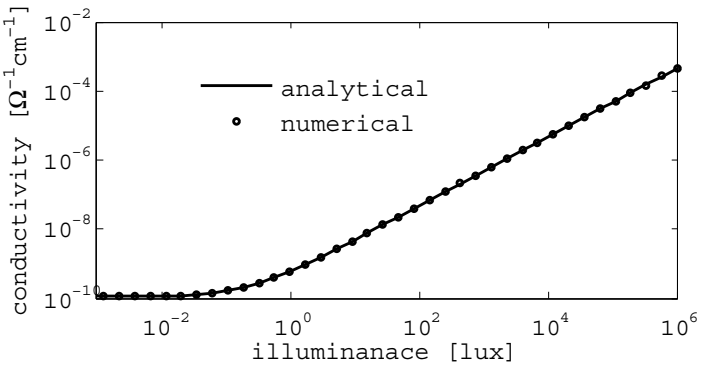

Figure 3. The mean conductivity, $\overline{\sigma}$, of an a-Si:H photoresistor versus illuminance, a simulation done for a $0.5\,\mu$m thick photoresistor ($\ell = 0.5\,\mu$m). The illumination is composed of monochromatic light with photon wavelength of $\lambda = 555\,$nm (green light). $\overline{\sigma}$ increases linearly with illuminance for levels greater than 1 lux. Therefore, this film is suitable for imaging over the range of human photopic vision, about 3 to $3 \cdot 10^5$ lux

4.3 Simulation results

The operating conditions and material parameters that were used in the simulation are given in Table 1. The simulation was performed for monochromatic light with $\lambda = 555\,$nm (green light). This wavelength represents the point where the photopic (color) vision of the human eye has maximum sensitivity, and it allows easy relation of Φ_0 to units used in imaging science to specify illuminance, such as lux. 10^{-3} lux is the amount of light one can measure outdoors on a cloudy night. In typical room/office conditions, the illuminance is in the range of 10^2 to 10^3 lux. On bright sunny days, the outdoors illuminance reaches about 10^5 lux. Color vision of the human eye starts at about 3 lux.

Fig. 3 shows the mean conductivity, $\overline{\sigma}$, of the a-Si:H layer versus illuminance. The calculation was performed for a $0.5\,\mu$m thick photoresistor. The material appears to be suitable for illuminance levels of above 1 lux, which covers the range of human color vision. The dark current at room temperature does not allow detection much below this value. The actual conductivities for the range where $\overline{\sigma}$ increases linearly with the illuminance (above 1 lux) are expected to be lower than those shown in the graph because, in a-Si:H, most excess charge carriers

Table 1. The operating conditions and material parameters used for the simulation.

Constant	Symbol	Value	Units
applied voltage	V_{ab}	1.5	V
photon flux	Φ_0	$1.23 \cdot 10^{15}$	$\mathrm{cm^{-2}\,s^{-1}}$
wavelength	λ	555	nm
light transmission factor	T	0.1	
scaled contact resistances	R'_a, R'_b	10	$\Omega\,\mathrm{cm^2}$
a-Si:H absorption coefficient @ 555 nm	α	10^5	$\mathrm{cm^{-1}}$
a-Si:H bimolecular recombination coefficient	α_r	$5 \cdot 10^{-10}$	$\mathrm{cm^3\,s^{-1}}$
a-Si:H dielectric constant	ϵ_r	8	
a-Si:H carrier concentrations	n_i, n_0, p_0	$6.257{\cdot}10^7$	$\mathrm{cm^{-3}}$
a-Si:H carrier mobilities	μ_n, μ_p	10, 1	$\mathrm{cm^2\,V^{-1}\,s^{-1}}$
a-Si:H diffusion coefficients	D_n, D_p	0.25875, 0.025875	$\mathrm{cm^2\,s^{-1}}$
a-Si:H recombination lifetimes	τ_n, τ_p	$4 \cdot 10^{-8}$, $3 \cdot 10^{-7}$	s

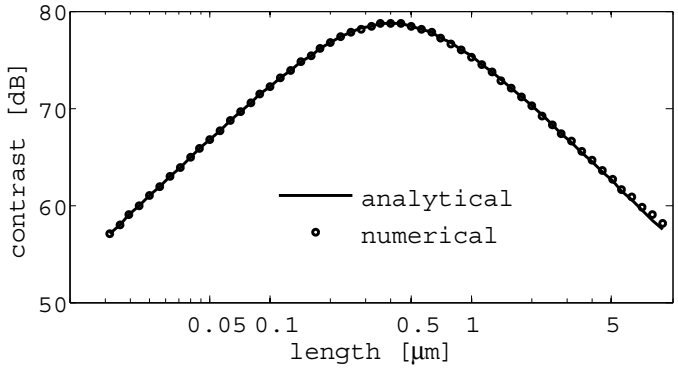

Figure 4. The contrast of the photodetector, β, versus the thickness of the intrinsic a-Si:H photosensitive layer. The contrast is defined as the ratio between J_{ph}, the current density under illumination, and J_{dk}, the current density in the dark. J_{ph} is calculated for a photon flux of $\Phi_0 = 1.23 \cdot 10^{15}\,\mathrm{cm}^{-2}\,\mathrm{s}^{-1}$ of monochromatic light with photon wavelength of $\lambda = 555\,\mathrm{nm}$, which is equivalent to illuminance of 3000 lux. A maximum is obtained at $l_{opt} = 0.4\,\mu\mathrm{m}$.

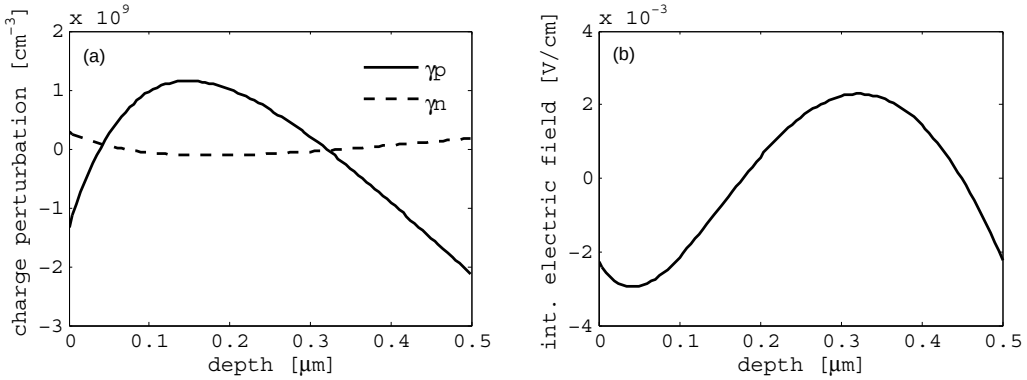

Figure 5. (a) The profile of the perturbation in the concentration of free charge carriers. (b) The profile of the internal electric field, E_{int}. Both (a) and (b) are calculated for a photodetector with a $0.5\,\mu$m thick a-Si:H layer, and illuminance of 3000 lux. The rest of the operating conditions and material parameters are given in Table 1. $\overline{\delta n} = 8.3176 \cdot 10^{11}\,\mathrm{cm}^{-3}$ and $E_{ext} = 1.8911 \cdot 10^4\,\mathrm{V/cm}$ for these conditions. Therefore, $\gamma_p, \gamma_n \ll \overline{\delta n}$ and $E_{int} \ll E_{ext}$.

are trapped in the bulk[11] and, therefore, do not contribute to the photoconductivity. A better approximation is expected once the multi-level trap model is incorporated into the recombination process. However, the magnitude of the dark current and the working range of the device should remain the same.

Fig. 4 gives the contrast, β, versus the thickness of the semiconductor layer, ℓ. It shows that there is an optimal thickness, ℓ_{opt}, for which the ratio of the photocurrent to the dark current is maximal, which is the main point of this paper. The simulation compares J_{ph} under illuminance at 555 nm (green light) of 3000 lux to J_{dk}; a maximum is obtained for $\ell_{opt} = 0.4\,\mu$m. The profile of the perturbation in the concentration of the charge carriers in the bulk is presented in Fig. 5(a), and the internal electric field, which is developed because of these perturbations, is shown in Fig. 5(b). These quantities were calculated by the iterative numerical method for a $0.5\,\mu$m thick a-Si:H layer. The mean value of the free charge carriers for these conditions is $\overline{\delta n} = 8.3176 \cdot 10^{11}\,\mathrm{cm}^{-3}$, and the external field is $E_{ext} = 1.8911 \cdot 10^4\,\mathrm{V/cm}$. Therefore, $\gamma_p, \gamma_n \ll \overline{\delta n}$ and $E_{int} \ll E_{ext}$.

5. DISCUSSION

It is important to check whether the simulation results agree with measured values. Since we could not find published experimental results for the problem as specified, we looked at published structures of similar a-Si:H photodetector devices. We were only interested in designs similar to the configuration given in this work, e.g. where the electric field was parallel to the direction of illumination. Table 2 gives details on the thicknesses

Table 2. This table shows the thicknesses of the layers in PECVD a-Si:H photodetectors, as published by different groups. All devices were used or tested in the visible range. The thickness of the intrinsic layer, which is the most important layer for the conversion of light into electrical signals, ranges between 0.25 and 2 μm.

Reference	Device	Thickness of Layers		
		p	i	n
Lulé *et al.*[3]	n-i-p TCO structure deposited on CMOS die for image sensor built in TFA technology	20 nm	1350 nm	30 nm
Hayama[12]	metal i-p TCO structure deposited on glass substrate for detection of light at 570 nm in stripe-type contact image sensor	10 nm	2000 nm	
Ng *et al.*[13]	metal n-i-p TCO structure deposited on polyethylene naphthalate substrate for thin-film-transistor flexible image sensor	10 nm	$\geq$ 600 nm	70 nm
Caputo *et al.*[14]	TCO n-i-p metal structure deposited on glass substrate for detection of light at 514 nm in chromatography system	20 nm	250 nm	70 nm
Vygranenko *et al.*[15]	metal n-i-p TCO structure deposited on glass and stainless-steel foil substrate for flexible image sensor	30 nm	500 nm	30 nm

of different layers for several a-Si:H photodetectors, which were fabricated by different groups. All the devices were either designed or tested in the visible band. The processes of generation and transportation of free charge carriers, which are later collected in the contacts, mainly occur in the intrinsic layer. As seen in Table 2, the thickness of the intrinsic layer in the published works ranges from 0.25 to 2 μm.

According to our simulation results, the maximum contrast is obtained when $\ell = 0.4\,\mu$m. However, it seems that a-Si:H photodetectors are usually fabricated with thicker i-layers. Assuming that our model sufficiently describes the behavior of a real a-Si:H based photodetector, one should note that we chose to optimize the structure for maximal contrast. One may choose a different criteria for device optimization, e.g. quantities that relate to the noise performance of the photodetectors, such as noise-equivalent-power (NEP) or detectivity (D*). These parameters may be calculated using the same method presented in this work, and may result in a different ℓ_{opt}. It is also possible that no optimization was performed prior to the design. Among the five mentioned works, only Ng *et al.*[13] reported a trial to reach optimization. They tested films with 600 and 1200 nm thick i-layers, and concluded that even though the thinner i-layers had the same density of defects as the thicker ones, the probability of recombination of free charge carriers due to these defects was smaller in the thinner films.

6. CONCLUSION

We have presented a new approach to solve the governing equations of charge carriers in a semiconductor. An analytical and numerical solution have been derived, which are based on different boundary conditions than those found in the literature. Our boundary conditions follow simply from Kirchoff's voltage law, charge neutrality, and generation-recombination balance. Moreover, we formulate excess charge carrier concentrations using local perturbation, which leads to efficiencies in the solution process. Furthermore, the approach is applied to optimize a photodetector structure for vertically-integrated CMOS image sensors. The simulation results, which were based on material parameters of a-Si:H, show that an optimal thickness exists that maximizes contrast. They also show that the differences between the analytical and numerical solutions are very small. Therefore, the analytical solution is quite accurate, and can be used to explain the maximum. If the a-Si:H layer is made too

thin, the device is dominated be the contact resistances. If it is made too thick, excess charge carriers spread out too thinly and so conductivity is hardly improved. Our model finds a maximum when the a-Si:H layer is $0.4\,\mu$m thick. However, experimental results will be needed to confirm the model or to suggest how it needs to be revised.

ACKNOWLEDGMENTS

The authors gratefully acknowledge the support of Alberta Ingenuity and the Natural Sciences and Engineering Research Council of Canada.

REFERENCES

[1] Kavusi, S., Kakavand, H., and Gamal, A. E., "Quantitative study of high dynamic range sigma delta-based focal plane array architectures," *Proceedings of the SPIE* **5406**, 341–350 (2004).

[2] Wong, H., "Technology and device scaling considerations for cmos imagers," *IEEE Trans. Electron Devices* **43**, 2131–2142 (1996).

[3] Lule, T., Schneider, B., and Bohm, M., "Design and fabrication of a high-dynamic-range image sensor in tfa technology," *IEEE J. of Solid-State Circuits* **34**, 704–711 (1999).

[4] Burns, J. A., Aull, B. F., Chen, C. K., Chen, C., Keast, C. L., Knecht, J. M., Suntharalingam, V., Warner, K., Wyatt, P. W., and Yost, D. W., "A wafer-scale 3-d circuit integration technology," *IEEE Trans. Electron Devices* **53**, 2507–2516 (2006).

[5] Bai, Y., Bajaj, J., Beletic, J. W., Farris, M. C., Joshi, A., Lauxtermann, S., Petersen, A., and Williams, G., "Teledyne imaging sensors: silicon cmos imaging technologies for x-ray, uv, visible and near infrared," *Proceedings of the SPIE* **7021**, 702102 (2008).

[6] McKelvey, J. P., [*Solid state and semiconductor physics*], Harper and Row, New York (1966).

[7] Mari, A. D., "An accurate numerical steady-state one-dimensional solution of the p-n junction," *Solid-State Electronics* **11**, 33–58 (1968).

[8] Gummel, H. K., "A self-consistent iterative scheme for one-dimensional steady state transistor calculations," *IEEE Trans. Electron Devices* **11**, 455–465 (1964).

[9] Sirbu, D., Skorka, O., and Joseph, D., "Simulation of Photodetectors in Hybrid Image Sensors," tech. rep., University of Alberta (2007). http://www.ece.ualberta.ca/∼djoseph/.

[10] Sakata, I. and Hayashi, Y., "Theoretical analysis of trapping and recombination of photogenerated carriers in amorphous silicon solar cells," *Appl. Phys. A* **37**, 153–164 (1985).

[11] Hack, M. and Shur, M., "Physics of amorphous silicon alloy p-i-n solar cells," *J. Appl. Phys.* **58**, 997–1020 (1985).

[12] Hayama, M., "Characteristics of p-i junction amorphous silicon stripe-type photodiode array and its application to ccontact image sensor," *IEEE Trans. Electron Devices* **37**, 1271–1279 (1990).

[13] Ng, T. N., Lujan, R. A., Sambandan, S., and Street, R. A., "Low temperature a-si:h photodiodes and flexible image sensor arrays patterned by digital lithography," *Appl. Phys. Lett.* **91**, 063505 1–3 (2007).

[14] Caputo, D., Ceccarelli, M., de Cesare, G., Intrieri, R., Manetti, C., Nascetti, A., and Scipinotti, R., "Chromatography system based on amorphous silicon sensor," *J. Non-Cryst. Solids* **354**, 2615–2618 (2008).

[15] Vygranenko, Y., Kerr, R., Kim, K. H., Chang, J. H., Striakhilev, D., Nathan, A., Heiler, G., and Tredwell, T., "Segmented amorphous silicon n-i-p photodiodes on stainless-steel foils for flexible imaging arrays," *Mater. Res. Soc. Symp. Proc.* **989**, 0989–A12–02 (2007).